GRIFFITH UNIVERSITY

Solar-Driven Atmospheric Water Production Through Hierarchically Ordered Porous Carbon for Self-Sustaining Green Hydrogen Production

Author

Fu, Bo, Zhang, Jifang, Robinson, Neil, Zhang, Zhen, Zhu, Zhengju, Dong, Mengyang, Zhang, Xinyuan, Kang, Jian, Michalski, Paul, Zhao, Zeyang, Ji, Jiapeng, Xu, Yiming, Zhang, Kaidi, Wang, Xinyu, Chen, Shan, et al.

Published

2025

Journal Title

Advanced Materials

Version

Version of Record (VoR)

DOI

10.1002/adma.202511336

Rights statement

© 2025 The Author(s). Advanced Materials published by Wiley-VCH GmbH. This is an open access article under the terms of the Creative Commons Attribution-NonCommercial-NoDerivs License, which permits use and distribution in any medium, provided the original work is properly cited, the use is non-commercial and no modifications or adaptations are made.

Downloaded from

https://hdl.handle.net/10072/439111

Funder(s)

ARC

Grant identifier(s)

DP200100965

Griffith Research Online
https://research-repository.griffith.edu.au

Check for updates

ADVANCED MATERIALS
www.advmat.de

Solar-Driven Atmospheric Water Production Through Hierarchically Ordered Porous Carbon for Self-Sustaining Green Hydrogen Production

Bo Fu, Jifang Zhang, Neil Robinson, Zhen Zhang, Zhengju Zhu, Mengyang Dong, Xinyuan Zhang, Jian Kang, Paul Michalski, Zeyang Zhao, Jiapeng Ji, Yiming Xu, Kaidi Zhang, Xinyu Wang, Shan Chen, Haolan Xu, Porun Liu,* Huajie Yin,* and Huijun Zhao**

Green hydrogen production by proton exchange membrane water electrolysis (PEMWE) powered by clean energy is a promising and environmentally friendly technology. However, it relies on a high-purity water source, which is limited in regions facing water scarcity. Here, a coupled self-sustaining solar-enabled system is reported that couples atmospheric water harvesting with PEM water electrolysis (AWH-PEMWE), offering a novel pathway for clean water generation and green hydrogen production. The atmospheric water harvester (AWH) component utilizes N and O co-doped hydrophilic ordered porous carbon, engineered with an interconnected hierarchical porous structure with prosperous channels for efficient mass transport. It enables effective interfacial solar evaporation for water release, achieving a record-high water harvesting capacity of 0.49 L kg^{-1} h^{-1} at 40% relative humidity (RH). During outdoor tests, the AWH-PEMWE system reaches a peak green hydrogen production rate of 204 mL h^{-1} at midday using only atmospheric water as feedstock. Remarkably, the system remains operational under ultra-low humidity conditions down to 20% RH, addressing the challenge of water availability in arid environments. Importantly, the system operates without the need for carrier gases or external energy input accessories, enabling a fully solar-driven process with zero carbon emission throughout the hydrogen production cycle.

1. Introduction

Proton exchange membrane water electrolysis (PEMWE) is a highly efficient and environmentally friendly technology for green hydrogen production, offering advantages such as high-purity hydrogen output, rapid response, and compact system design. However, its dependence on highly purified water as a feedstock poses a significant challenge to wide deployment, especially in regions where freshwater resources are scarce. Integrating PEMWE with a self-sustaining, solar-driven atmospheric water harvesting (AWH) system presents a compelling solution to concurrently address energy and water shortages, particularly in arid and semi-arid environments.[1] This hybrid system leverages interfacial solar evaporation to extract pure water from atmospheric moisture absorbed during nocturnal cycles, which subsequently feeds the PEMWE for hydrogen production.[2–7] Realization of such a sustainable system critically depends on the

B. Fu, M. Dong, Y. Xu, K. Zhang, X. Wang, P. Liu, H. Zhao
Centre for Catalysis and Clean Energy
Gold Coast Campus
Griffith University
Gold Coast, Queensland 4222, Australia
E-mail: p.liu@griffith.edu.au; h.zhao@griffith.edu.au

B. Fu, J. Zhang, Z. Zhang, X. Zhang, J. Kang, S. Chen, H. Yin
Key Laboratory of Materials Physics
Centre for Environmental and Energy nanomaterials
Anhui Key Laboratory of Nanomaterials and Nanotechnology
CAS Center for Excellence in Nanoscience
Institute of Solid State Physics
Hefei Institutes of Physical Science
Chinese Academy of Sciences
Hefei 230031, China
E-mail: yinhj@issp.ac.cn

N. Robinson
School of Chemistry and Chemical Engineering
Queen's University Belfast
Belfast, Northern Ireland BT9 5AG, UK

© 2025 The Author(s). Advanced Materials published by Wiley-VCH GmbH. This is an open access article under the terms of the Creative Commons Attribution-NonCommercial-NoDerivs License, which permits use and distribution in any medium, provided the original work is properly cited, the use is non-commercial and no modifications or adaptations are made.

DOI: 10.1002/adma.202511336

development of high-performance AWH materials that exhibit rapid water sorption-desorption kinetics and efficient photothermal conversion under solar irradiation.

Carbon-based materials have emerged as particularly promising candidates for solar-driven AWH due to their intrinsic photothermal properties, high surface area, porosity, and chemical stability. In contrast to non-photothermal AWH sorbents that require external heat sources for water release, carbon-based materials can directly harness solar energy to drive water desorption.[8–12] The conventional carbon-based sorbents, such as graphene oxide, activated carbon and activated carbon fibers have demonstrated the feasibility of water release via interfacial solar evaporation.[13–18] However, their water harvesting capacity and adsorption kinetics remain inadequate for practical applications. To overcome these limitations, one strategy is to introduce hydrophilic functional groups to increase the number of active sites for moisture capture.[19–21] Besides the water affinity, the relatively low water-accessible surfaces and insufficient pore connectivity also constrain the AWH capacity and kinetics. Another approach is to engineer hierarchical porous structures and vertically aligned structures to enhance water-accessible surface area and facilitate efficient mass transport.[22–25] However, the state-of-the-art carbon sorbents primarily rely on micro- or mesopores, highlighting the need for optimized carbon materials with elaborately designed interconnected hierarchical pore structures and hydrophilic surfaces.

Herein, we report a zeolitic imidazolate framework (ZIF-8)-derived carbon material (ZC) engineered with oxygen-containing functional groups and a hierarchically ordered porous structure, as an efficient photothermal AWH absorber. Among the synthesized materials with different pores, the ordered carbon with 270 nm pores demonstrated superior water harvesting capacity compared to the bulky ZC counterparts without hierarchical pores, owing to its enhanced porosity and surface accessibility. Moreover, the incorporation of hydrophilic functional groups significantly improved moisture uptake, achieving a high water harvesting capacity of ≈0.49 L kg^{-1} h^{-1} at 40% RH. Remarkably, the hydrophilic ordered porous carbon (HOC) exhibited excellent light absorption, high specific surface area, and outstanding photothermal performance, enabling a solar evaporation rate of ≈0.72 L kg^{-1} h^{-1} under AM 1.5G illumination. When coupled with a solar-powered PEMWE, the pure water released from the HOC-based AWH sustained green hydrogen production at a peak rate of 204 mL h^{-1} without requiring additional water or power input. This work demonstrates a novel and practical approach to solar-driven green hydrogen production, establishing a promising pathway for deployment in water-constrained regions and advancing the development of carbon-neutral hydrogen energy systems.

Z. Zhu
Key Laboratory for Ultrafine Materials of Ministry of Education
Shanghai Engineering Research Center of Hierarchical Nanomaterials
School of Materials Science and Engineering
East China University of Science and Technology
Shanghai 200237, China
P. Michalski
Department of Chemical and Biological Engineering
Monash University
Clayton, Victoria 3800, Australia
Z. Zhao
Queensland Alliance for Environmental Health Sciences
The University of Queensland
Brisbane, Queensland 4102, Australia
J. Ji
Institute of Technology for Carbon Neutrality
Shenzhen Institute of Advanced Technology
Chinese Academy of Sciences
Shenzhen, Guangdong 518055, China
H. Xu
Future Industries Institute
UniSA STEM
University of South Australia
Mawson Lakes Campus
Adelaide, South Australia 5095, Australia
E-mail: haolan.xu@unisa.edu.au

2. Results and Discussion

2.1. Properties of Hydrophilic Ordered Porous Carbon

As illustrated in Figure S1 (Supporting Information), the ordered porous carbon with excellent hydrophilicity was first synthesized according to our previous work.[19,26] Briefly, the ZIF-8 precursor was impregnated in the self-assembly 3D-ordered polystyrene spheres (PSs, 270 nm in diameter) template for the growth of PS-embedded ZIF-8 crystals (ZIF-8@PS). The obtained ZIF-8@PS was subjected to pyrolysis to decompose PSs and carbonize ZIF-8, resulting in the uniformly sized and cuboctahedron-shaped ordered carbon materials (OC270). Two strategies were applied to introduce oxygen-containing functional groups (OFGs) to improve hydrophilicity. The OC270 sample treated with a mixed acid (H_2SO_4 + HNO_3) aqueous solution was denoted as OC270-A, while the one activated by direct calcination in air was named as HOC270. To explore the effect of the pore size on solar-driven AWH, we also synthesized samples with 180 and 400 nm macropores followed by calcination, denoted as HOC180 and HOC400, respectively. The ZC sample was obtained without the use of PSs template or surface modification (Figure S2, Supporting Information).

Scanning electron microscopy (SEM) image of the HOC samples revealed a cuboctahedron-shaped structure with 3D-ordered microporous cells interconnected by well-controlled pores (**Figure 1**a,b; Figures S3–S5, Supporting Information), confirming the successful synthesis of the ordered porous structure. Transmission electron microscopy (TEM) and high-resolution transmission electron microscopy (HRTEM) of the HOC270 sample also confirmed the interconnected pore structure (Figure 1c; Figure S6, Supporting Information). The porous features were further analyzed by N_2 adsorption-desorption isotherms (Figure 1d), which confirmed the presence of micropores with diameters of 0.82, 1.12, 1.41, and 1.76 nm. The measured Brunauer-Emmett-Teller (BET) surface area was 1052.2 m^2 g^{-1}. In comparison, the ZC particles prepared without the PSs template did not display apparent meso-macropores, confirming the crucial role of the PSs template in constructing the ordered hierarchical porous structure (Figure S7, Supporting Information). It is noted that calcination treatment (HOC270) did not remarkably change the surface area (994.3 m^2 g^{-1}) while the acid treatment (OC270-A) reduced the surface area to 795.4 m^2 g^{-1}.

© 2025 The Author(s). Advanced Materials published by Wiley-VCH GmbH

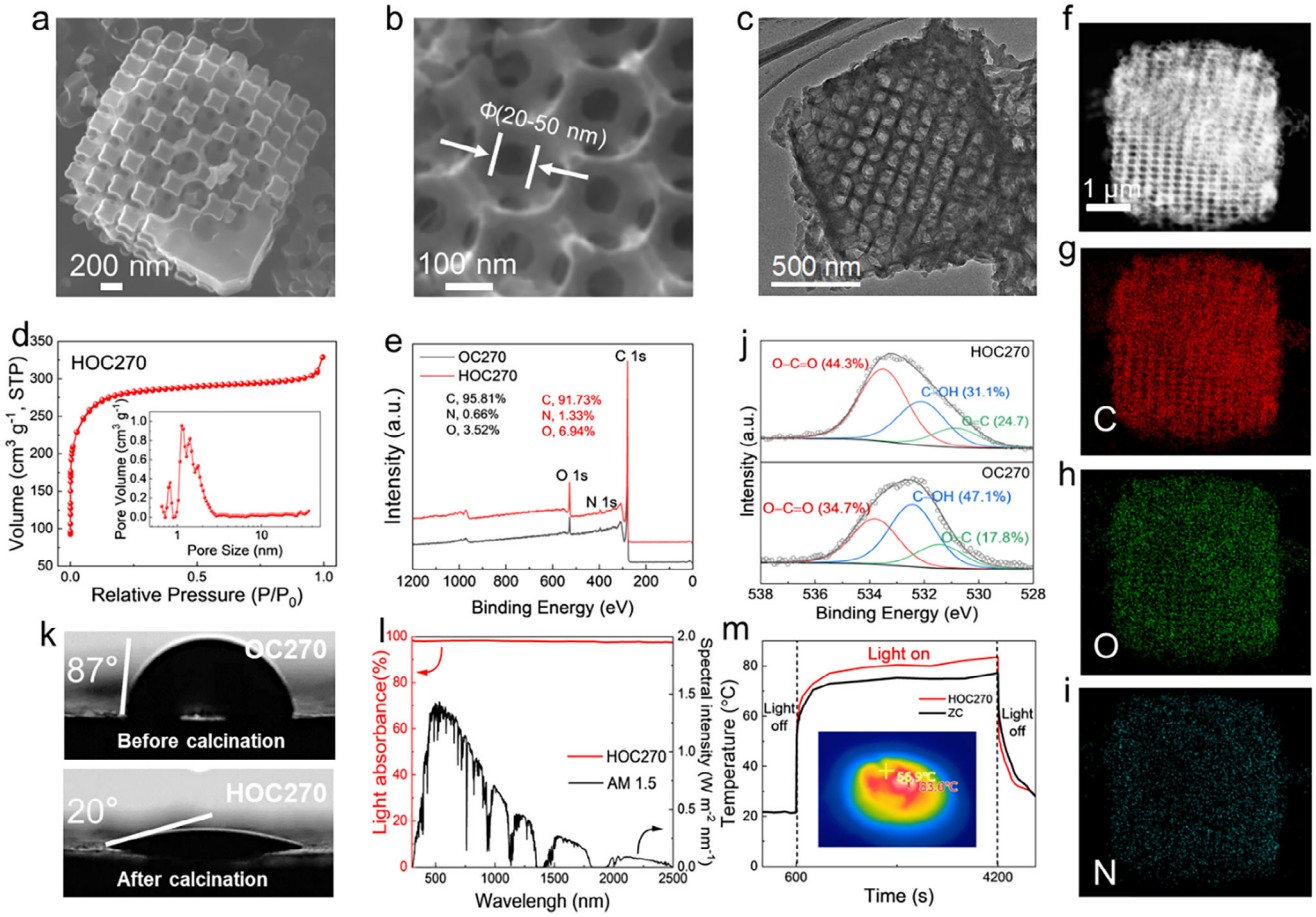

Figure 1. Structure and compositional analyses of ordered porous carbon. a) SEM image of HOC270. b) SEM image of the connected mesopores and macropores. c) TEM image of the HOC270 sample with an interconnected pore structure. d) N_2 adsorption-desorption isotherms and pore-size distributions of HOC270. e) XPS data of the samples before and after calcination in air. f–i) HAADF-STEM and the corresponding EDS mapping images of C, N, and O of HOC270. j) High resolution O 1s XPS spectra of OC270 and HOC270. k) Water contact angle variation of the sample before and after calcination. l) UV–vis–NIR absorption performance measured by the integrated sphere module. m) Temperature profile and Infrared images of ZC and HOC270 sample under one-sun illumination.

The crystal and structural properties of the HOC270 were characterized by X-ray diffraction (XRD) and Raman spectroscopy which indicated a typical disordered graphitic carbon structure (Figure S8, Supporting Information), consistent with the results of HRTEM. The X-ray photoelectron spectroscopy (XPS) spectra (Figure 1e) confirmed the presence of C, N, and O in the HOC270, while the HAADF-STEM image and energy dispersive spectroscopy (EDS) mapping (Figure 1f–i) revealed the uniform distribution of C, O, and N elements. The XPS survey spectra of OC270 and HOC270 indicated that the surface O was significantly increased from 3.52% to 6.94% after the calcination. The high-resolution O 1s XPS spectra of both samples depicted three OFGs: carbonyl (C═O) at 531.4 eV, hydroxyl (C—OH) at 532.5 eV and ester (O–C═O) group at 533.8 eV (Figure 1j). Before treatment, surface oxygen species consisted of ≈47.1% hydroxyl (C—OH), ≈34.7% carboxylate (O–C═O), and ≈17.8% carbonyl (C═O) groups. After air calcination, the overall oxygen content increased, and the distribution shifted to ≈31.1% C—OH, ≈44.3% O–C═O, and ≈24.7% C═O. In the Near Edge X-Ray Absorption Fine Structure (NEXAFS) spectra (Figure S9, Supporting Information), the absorption edge step at 531.8 eV confirmed that compared to OH, the total oxygen of HOC270 increased by ≈16.4%. In addition, the Fourier-transform infrared spectroscopy (FT-IR) spectrum (Figure S10, Supporting Information) also showed a significant increase in OFGs in HOC270, consistent with the XPS and NEXAFS results. The peaks at 1552 and 1723 cm^{-1} can be allocated to C═O vibrations in COOH groups. Another strong band located at 1189 cm^{-1} could be assigned to the stretching vibration of C–O. Besides, the peaks at 3607 cm^{-1} can be allocated to N–H stretch. The N 1s XPS spectrum (Figure S11, Supporting Information) of HOC270 revealed the presence of pyridinic N (≈398.5 eV) and graphitic N (≈401.0 eV). All these results collectively confirmed a significant increase in surface functional groups with high water affinity in the hierarchically ordered porous carbon after direct calcination in the air.[27]

Due to the rich OFGs on the surfaces, the hydrophilicity of the obtained HOC270 was remarkably enhanced compared to that of OC270. The water contact angle decreased significantly from 87° to 20° after calcination (Figure 1k). The light absorbance and photothermal response of HOC270 were investigated to assess

© 2025 The Author(s). Advanced Materials published by Wiley-VCH GmbH

its response to solar irradiation. As shown in Figure 1l, due to the unique ordered hierarchical porous structure, HOC270 exhibited broad light absorption ranging from 300 to 2500 nm with an average absorbance of over 98%. As a result, HOC270 exhibited a rapid temperature increase under one-sun illumination (1 kW m^{-2}). Within 30 s, its temperature in the air rose swiftly to 60.6 °C, then reached 83.6 °C after 5 min (Figure 1m). This fast photothermal response and efficient solar-to-thermal energy conversion will facilitate the rapid water release via interfacial solar evaporation, and AWH cycles.

2.2. AWH Performance and In Situ Investigation by LF-NMR Relaxation

The AWH performance of the HOC samples with different macroscopic pore sizes and surface modifications was measured at 22°C and 20%–50% RH. As illustrated in **Figure 2a**, OC270 showed more significant water uptake than conventional ZC without macroscopic pores, signifying the crucial role of the hierarchically porous structure in promoting the water uptake capacity. More importantly, the results clearly demonstrated that the improvement of surface hydrophilicity by calcination approach (i.e., HOC samples) is more conducive to the enhanced AWH performance (Figure 2a). Apart from hydrophilicity, pore size also remarkably affected the AWH performance. Among HOC samples with different pore sizes, HOC270 with medium-sized macro pores delivered the best water uptake performance under all RH conditions investigated and was thus employed in further study.

Within the RH ranges investigated, it was evident that HOC270 absorbed moisture at a rapid rate in the first 30 min, then reached saturation in 1 h (Figure 2b). The rapid adsorption can be attributed to the hierarchical porous structure and the abundant hydrophilic water binding sites on the surface. Furthermore, the isotherm curve (Figure S12, Supporting Information) shows a Type V sorption behavior, indicative of moderate hydrophilicity and capillary condensation in the hierarchical porous structure. Under one sun irradiation, the captured water can be released rapidly from HOC270 via interfacial solar evaporation due to the fast and efficient photothermal response. In addition, the abundant micropores are beneficial for light absorption and can promote the solar evaporation rate.[35] Unlike the conventional absorbents, which are composed of separated AWH and thermal layers and require extra energy input for water release, the HOC270 is activated by solar energy without the need for external accessories for energy input, featuring an integrated design, high energy utilization efficiency and low operation cost. The multiple water harvest and release tests of HOC270 confirmed its excellent cyclability and stable performance (Figure 2c; Figure S13, Supporting Information). Noteworthily, among the state-of-the-art solar-driven AWH materials, our HOC270 achieved a superior water uptake rate under 20%–50% RH range (Figure 2d).[36–49]

To further investigate the AWH process, in situ low-field (LF) ^{1}H NMR relaxation experiments were conducted to measure the transverse relaxation time (T_2) characteristics of water during AWH using HOC270 (Figure 2e). Such measurements provide rapid and non-invasive approach to characterize the fluids confined within functional porous materials,[50] enabling the investigation of the kinetics of vapor/moisture uptake by the carbon materials.[51] The observed relaxation rates of water within such systems can be expressed as $T_2^{-1} \approx \rho S/V$, where S/V is the surface-to-volume ratio of the confining pore structure and ρ is the surface relaxivity of the material/fluid interface, which acts as a scaling factor between pore size and observed relaxation times;[52,53] in the present case this term will be dominated by hydrogen-bond-mediated adsorption interactions between adsorbed water and the hydrophilic groups on the carbon surfaces.[52,54] The observed relaxation times of water confined within carbon pores therefore are shorter than those of the unrestricted bulk water. Figure 2e showed time-resolved T_2 distributions obtained in situ with HOC270 subjected to humid air for 5–90 min. At short times, a single relaxation population was observed at short T_2 (≈3 ms), which was assigned to adsorbed water within the porous carbon structure (note resolution of multiple relaxation times associated with water within pores of different sizes is not possible here due to the low signal-to-noise ratio of the acquired data). This population clearly increased in intensity as a function of time exposure to water vapor, confirming uptake of water vapor by adsorption within the pore structures of HOC270 during this process. At 90 min of moisture capture, an additional relaxation population was observed at T_2 ≈3 s, characteristic of unrestricted water, indicating the existence of bulk water outside of the carbon material and hence the saturation of AWH, consistent with the kinetic AWH results in Figure 2b.

Based on the LF-NMR results, a schematic of AWH processes involving water cluster formation, growth, coalescence (transformation of interface), and filling in interconnected hierarchical pores of HOC270 was proposed (Figure 2f). At the beginning, water molecules are adsorbed onto the high-density OFG sites on the carbon surfaces. As the growth of large clusters requires a higher chemical potential, water uptake occurs progressively from smaller to larger pores.[28] When water adsorption proceeds, the hydrogen bonds of restricted water are established between functional groups and water molecules, which act as additional adsorption active sites and induce neighboring water vapor molecules bond with the previous layer of the adsorbed water layer.[29–31] The multilayer water adsorption proceeds through the hierarchical micro-meso-macroporous network via capillary condensation and eventually results in an encapsulated bulk water throughout the pores.

Compared with the previous AWH work based on carbon materials,[32] our hierarchically interconnected and ordered porous structure provides enhanced affinity with water molecules. The high surface area and excellent pore connectivity of the micro-meso-macro trimodal-porous structure render the HOC270 with high-density exposed water nucleation sites that facilitate water adsorption and cluster growth on the surfaces and pores.[28,33,34,55,56] In conventional carbon materials, the water uptake is close to equilibrium when water fully fills the micropores and mesopores. In contrast, the HOC270 with an interconnected micro-meso-macro porous structure enables efficient water diffusion and mass transfer thus facilitating continuous filling of water into the hierarchically constructed interconnected pores, boosting the water uptake capacity and rate. In addition, the elaborate calcination treatment successfully

© 2025 The Author(s). Advanced Materials published by Wiley-VCH GmbH

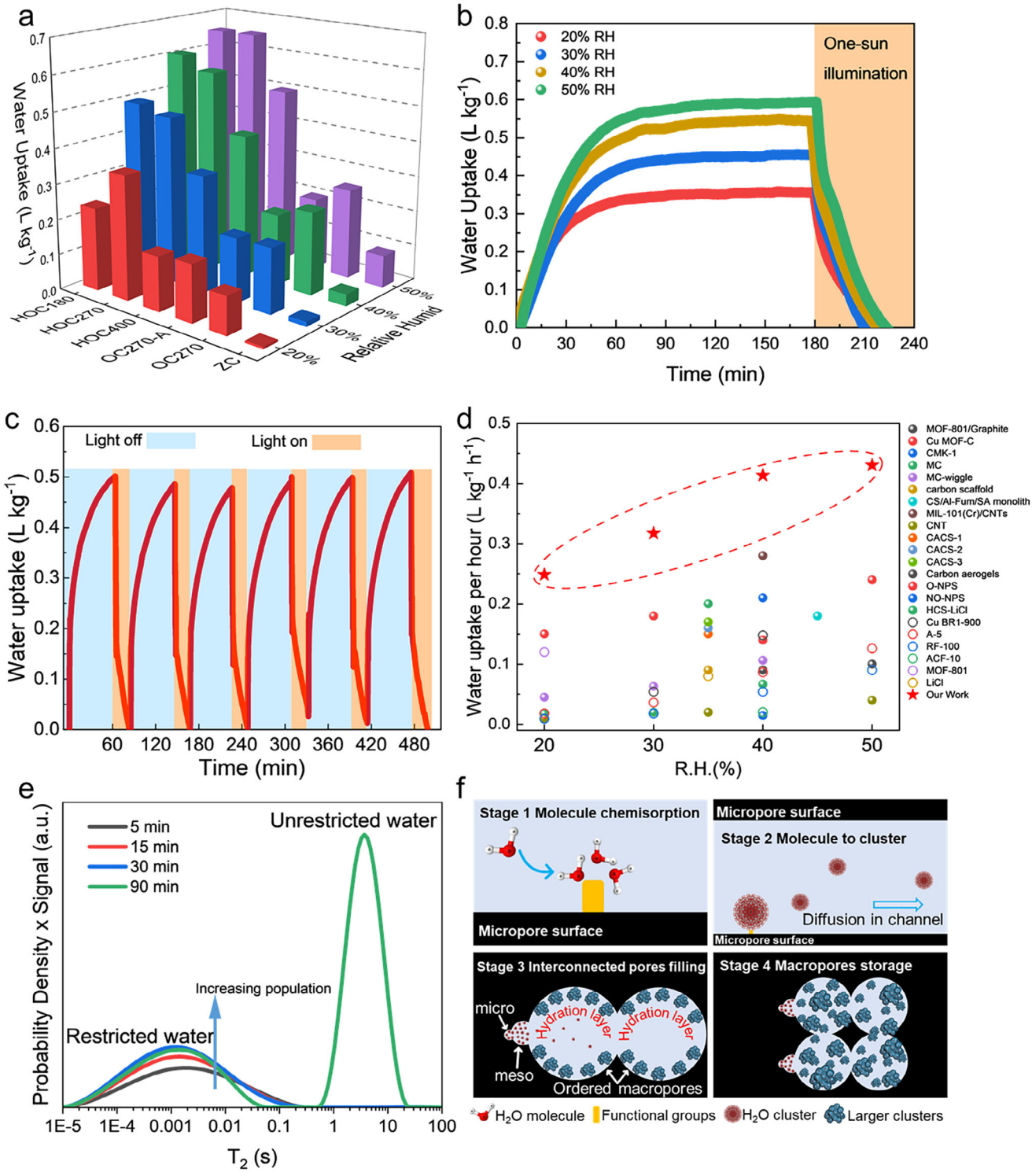

Figure 2. AWH performance of the obtained carbon samples. a) AWH performance of HOC (180, 270, and 400 nm pores) OC270-A, OC270, and ZC. b) AWH performance of HOC270 under 20%, 30%, 40%, and 50% RH, respectively. c) Water uptake cycling performances of HOC270 under 40% RH. d) Comparison of AWH performance of HOC270 and state-of-the-art absorbents. The hollow circles present absorbents without solar evaporation function, and the solid spheres present the solar-driven AWH materials.[2,28–34] e) In situ LF-NMR analysis of the variation of water state during the AWH period. f) Schematic diagram of water adsorption process on HOC270.

© 2025 The Author(s). Advanced Materials published by Wiley-VCH GmbH

introduced more OFGs on the surfaces while maintaining the hierarchical and ordered porous structure well. The enriched OFG binding sites on the surfaces are conducive to the initial water nucleation to promote the water adsorption process, leading to an outstanding AWH performance.[57,58] The introduction of hydrophilic oxygen-containing functional groups (e.g., –COOH, –OH) reduces the nucleation energy barrier by stabilizing adsorbed water molecules via hydrogen bonding and promoting cluster formation at lower relative humidity.[59,60] This enhances the initial water uptake rate and facilitates faster moisture condensation within the hierarchical porous network.[59] It is noteworthy that acid oxidation treatment partially damages the hierarchically interconnected and ordered porous structure of OC270-A sample and jeopardizes its water uptake capacity, evidencing the essential role of the hierarchical porous structure. In summary, the rapid, cyclable, high-capacity water capture and release of HOC270 absorbent provides great promise for solar-driven green hydrogen production.

2.3. Atmospheric Water Harvesting PEM Electrolyzer

The integrated atmospheric water harvesting and electrolysis was realized through a custom-made AWH-PEMWE coupled device. As shown in **Figure 3**a, the electrolyzer consisted of a PEM with thermoforming catalysts on both sides, two air diffusion layers, a horizontal end plate (cathode side) and a modified end plate (anode side) with housing for loading HOC270 water sorbents and a transparent quartz window for solar illumination (Figure S14, Supporting Information). Room moisture was introduced into the housing of the modified end plate and absorbed by HOC270. After the water uptake, the HOC270 sorbents were illuminated by simulated sunlight through the quartz window to release the collected water. Due to the fast photothermal response of HOC270, the vapor was rapidly generated, with fogging observed in the anode housing within 1 min. After 2 min, larger water droplets were formed and observed on the surface of the quartz window (Figure 3b; Figure S15, Supporting Information). The system using pure water exhibited a higher current density (6.3 A at 2.0 V) compared to that using atmospheric water (2.8 A at 2.0 V). This difference is primarily attributed to the relatively lower ionic conductivity and possible trace impurities in the atmospheric water-derived feed. However, it is noteworthy that both systems display similar onset potentials (macroporous1.45 V), indicating that the intrinsic electrocatalytic behavior of the electrode materials remains unaffected (Figure S16a,b, Supporting Information). Notably, to achieve high performance of hydrogen production in general PEMWE, provision of circulating water moisture with a temperature of 60-80 °C is required. In our AWH-PEMWE setup, the hot moisture generated via interfacial solar evaporation eliminates the need to employ extra heating elements for the feed-in water for the PEMWE. The engineered hierarchical porous structure (micro–meso–macro) enhances both the surface area for water sorption and the channels for mass transport. The presence of macropores ensures fast vapor diffusion, while micropores and mesopores provide abundant active sites for moisture adsorption. The high porosity and ordered structure promote efficient light absorption and heat localization, which accelerates interfacial solar evaporation and enables rapid water release during the daytime. A faster water release rate means more consistent vapor supply to the PEMWE.

The operation of the AWH-PEMWE system can be divided into three steps. First, the HOC270 harvests water from the air. Then clean water is released by solar-driven vapor generation followed by an electrochemical hydrogen production step operated potentiostatically at 1.65 V (Figure 3c). During the water uptake cycles, the absorbent housing with the HOC270 was exposed to a flow of air (50 min), while the switch remained closed during the solar-driven vapor generation (10 min) and electrolysis step (1 h). Approximately 295.5 mL hydrogen can be collected in 60 min of electrolysis cycle (Figure 3d). In the electrolysis cycle (Figure 3e), constant hydrogen bubbles could be observed (Video S1, Supporting Information), and the hydrogen could be sustainably collected.

2.4. Solar-Driven/Powered AWH-PEMWE

The outdoor experiment was carried out to verify the practical operation of the coupled AWH-PEMWE for green hydrogen production under natural sunlight. As shown in **Figure 4**a, a solar panel (175 × 116 mm) was used to power the AWH-PEMWE with a small footprint (one-fourth of the solar panel). Similar to the experiment in the laboratory, the HOC270 in the coupled AWH-PEMWE device was saturated with water moisture by pumping the atmospheric air through the housing during the water uptake cycle for 50 min. Subsequently, during the electrolysis cycle, the PEMWE was fed by the water vapor released by interfacial solar evaporation using the reflected natural sunlight in a close setting for 10 min (Figure 4b). The AWH-PEMWE was tested from 8:00 a.m. to 4:00 p.m. in an open area in Southeast Queensland, Australia. The environmental parameters, the PEMWE real-time working parameters and the flow rate of generated hydrogen were simultaneously recorded.

During outdoor tests, the solar panel and solar power meter were placed horizontally without adjusting during the test, so the solar intensity varied with the solar zenith angle in a day which aligned well with the conditions during practical applications. As shown in Figure 4c, the working current and the hydrogen production rate reached their highest in the middle of the day when the strongest solar radiation was recorded at 0.77 kW m^{-2}. In the daytime, the environmental temperature varied from 22.0 to 28.8 °C and the relative humidity ranged from 33% to 60% during the experiment. The low relative humidity dominated most of the daytime, which was consistent with the humidity in the semi-arid area. Surprisingly, the environmental temperature and humidity did not strongly influence the rate of hydrogen production during the practical operation. The solar-to-vapor efficiency can achieve 45%–57% under different humidity (Figure S17, Supporting Information). Hence, our AWH-PEMWE device would be applicable in many semi-arid areas around the world.

Using the unique proton exchange membrane, the electrolyzer can produce hydrogen with high purity. Moreover, in contrast with the published research on conventional vapor electrolysis that deeply relies on carrier gases (N_2 or Ar), the AWH-PEMWE device can produce high-purity green hydrogen

© 2025 The Author(s). Advanced Materials published by Wiley-VCH GmbH

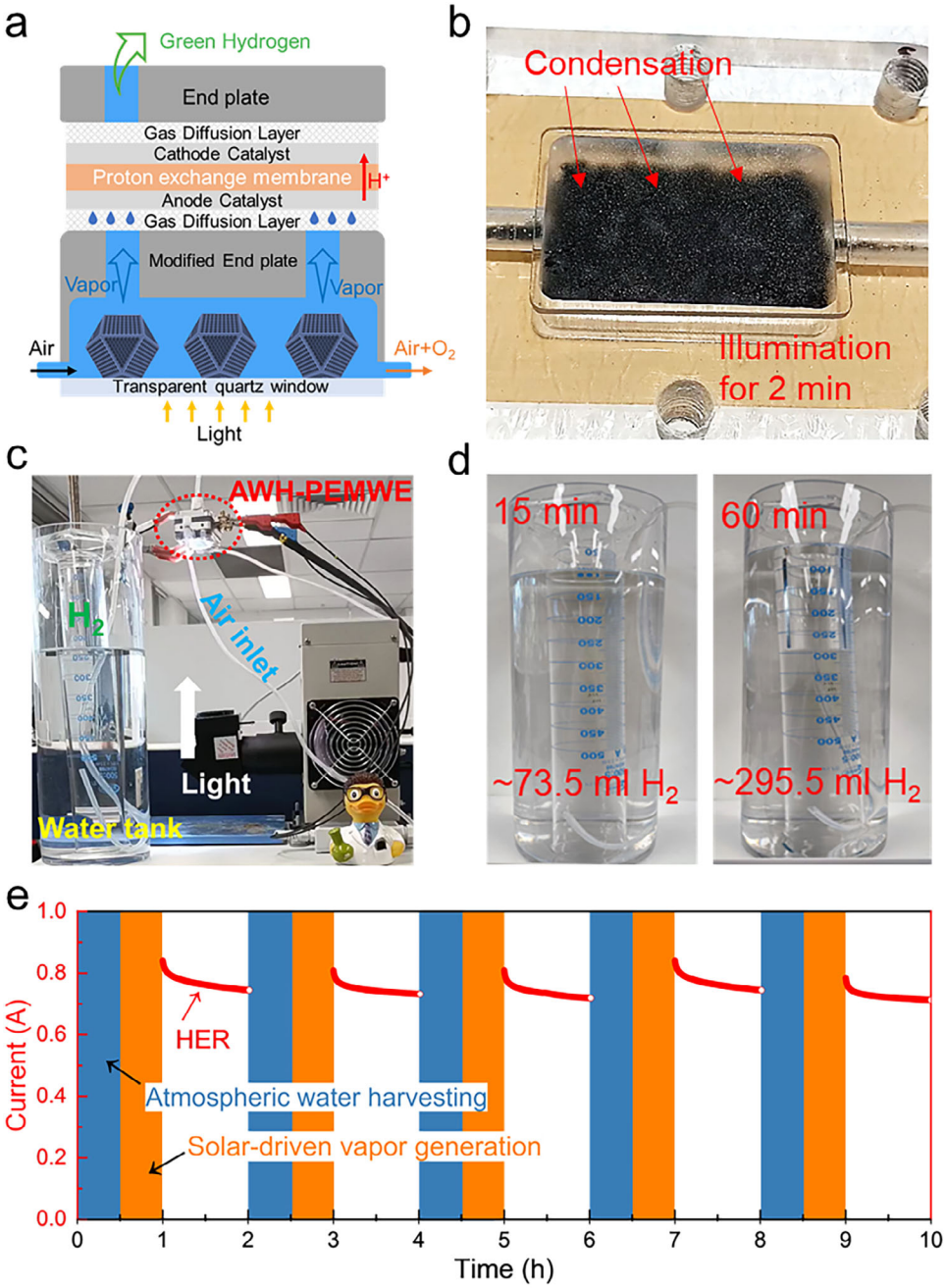

Figure 3. Water electrolysis fed by AWH. a) A schematic diagram of the AWH-PEMWE with pure water harvested and released from HOC270 sample. b) Photographs of the AWH experiment. Condensation can be observed on the window after illuminating for 2 min. c) The photo of AWH-PEMWE device under operation. d) Hydrogen production after 15 min and 1 h. e) Cycling test of the AWH-PEMWE. The cycle consists of a 30-min AWH step (blue) a 30-min solar-driven vapor generation to produce water vapor (orange) and water electrolysis of the photothermally generated water vapor (green).

without using any carrier gases, demonstrating attractive cost-effectiveness.[2,61–68] Owing to the rapid water adsorption and release kinetics, the AWH-PEMWE system ensures sufficient water availability, enabling significantly higher operating current and hydrogen production rates compared to all previously reported solar-driven vapor-phase water electrolysis systems (Figure 4d; Table S1, Supporting Information). The sorbents also show great promise for large-scale applications due to the cost-effective synthesis (Tables S2 and S3 Supporting Information). Moreover, in comparison to the required relatively high humidity conditions (>60%) in the literature, this AWH-PEMWE device is capable of harvesting moisture from lower humid environments (RH = 20 %) and producing green hydrogen. Our experimental results validate that the demonstrated AWH-PEMWE system can be deployed in an arid area with water scarcity.

© 2025 The Author(s). Advanced Materials published by Wiley-VCH GmbH

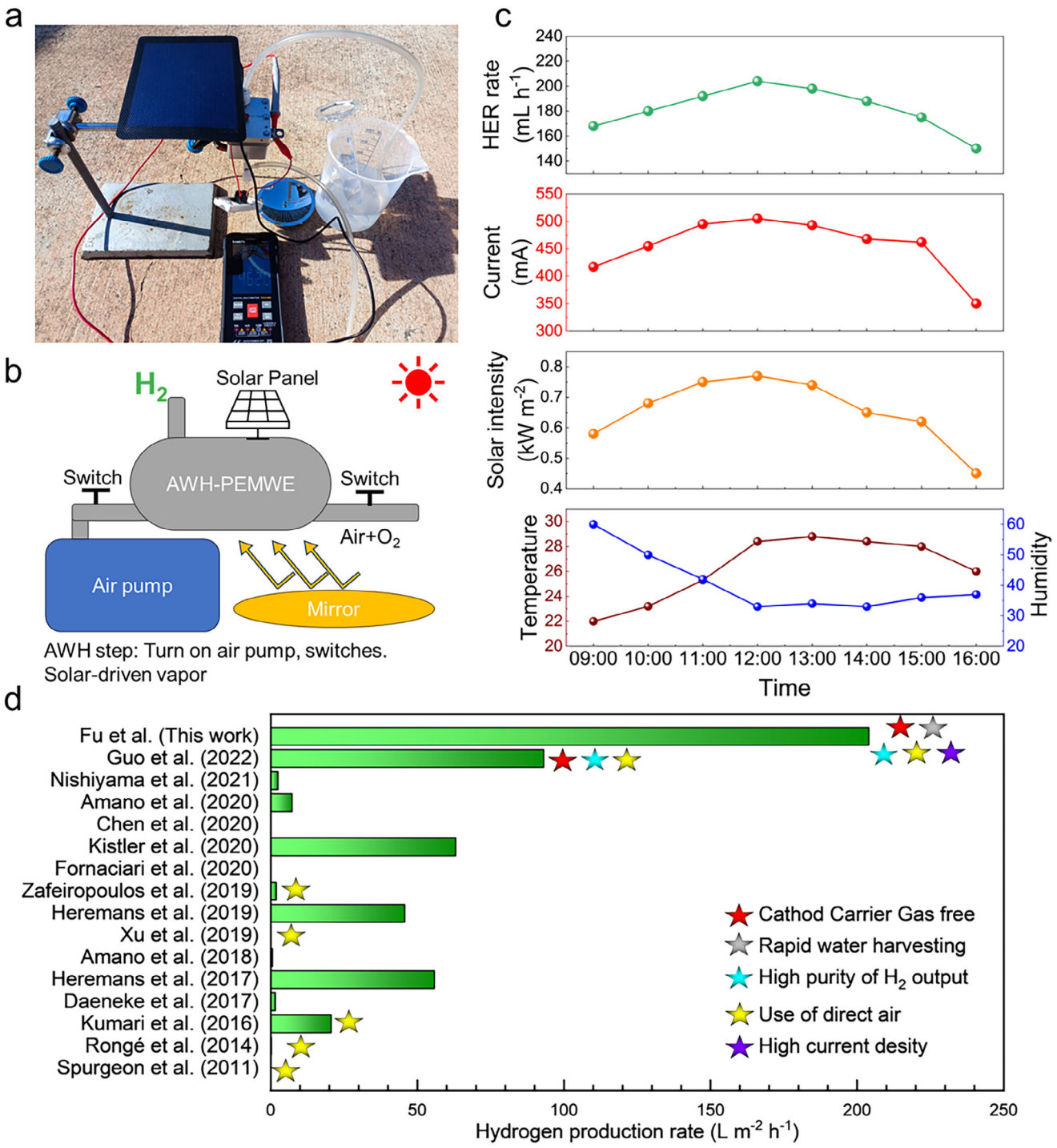

Figure 4. Outdoor Application of Solar-driven/powered AWH-PEMWE. a) Photo of the self-sustaining AWH-PEMWE system. b) Schematic of the self-sustaining AWH-PEMWE system. The green hydrogen production procedure: (1) Turn on the air pump and switches for AWH (50 min). (2) Turn off the switches and carry out solar-driven evaporation (10 min). (3). Turn on the switches and carry out HER (1h). c) Hourly hydrogen production rate, working status of PEM and corresponding atmospheric conditions. d) Comparisons between our AWH-PEM and other solar-driven water/vapor electrolysis reports.

© 2025 The Author(s). Advanced Materials published by Wiley-VCH GmbH

3. Conclusion

To solve the clean water and energy shortages for PEM electrolysis, we demonstrated a new pathway for producing green hydrogen via cascade solar-driven AWH and electrolysis. Due to the unique hierarchical and interconnected porous structure and rich OFGs our carbon materials achieved high moisture harvest capacity even under extremely low humidity (RH = 20%) and rapid vapor generation under one-sun illumination. After loading the HOC270 in an AWH-PEMWE device, the AWH and electrolysis processes can be conducted in one integrated device using solar energy. Pure hydrogen was quickly generated with high current without the need for electrolytes or carrier gas. Besides, the electrolyzer could also be powered with other renewable energy (wind energy, tidal energy, etc.) and is deployable in a natural environment. The demonstrated AWH-PEMWE coupled device exemplifies an environmentally friendly green hydrogen production avenue.

Supporting Information

Supporting Information is available from the Wiley Online Library or from the author.

Acknowledgements

The authors thank the financial support from the National Natural Science Foundation of China (52102197, 52102325), Collaborative Innovation Program of Hefei Science Center, CAS (2022HSC-CIP016), and Australian Research Council (DP200100965, DP210104010, DP230102504). N.R. acknowledges support from the Forrest Research Foundation and thanks Prof Mike Johns (University of Western Australia) for access to the NMR data processing software. The authors thank the Australian Synchrotron, a part of ANSTO, for NEXAFS measurements and Dr. Craig Stoppiello, Dr. Joseph Fernando, and Dr. Joseph Otte from The University of Queensland for the help with characterization.

Conflict of Interest

The authors declare no conflict of interest.

Data Availability Statement

The data that support the findings of this study are available in the supplementary material of this article.

Keywords

ordered porous carbon, self-sustaining hydrogen production, solar-driven water harvesting

Received: June 15, 2025
Revised: July 30, 2025
Published online:

[1] J. Guo, Y. Zhang, A. Zavabeti, K. Chen, Y. Guo, G. Hu, X. Fan, G. K. Li, *Nat. Commun.* **2022**, *13*, 5046.
[2] S. Kumari, R. Turner White, B. Kumar, J. M. Spurgeon, *Energy Environ. Sci.* **2016**, *9*, 1725.
[3] D. Tonelli, L. Rosa, P. Gabrielli, K. Caldeira, A. Parente, F. Contino, *Nat. Commun.* **2023**, *14*, 5532.
[4] W. Guan, C. Lei, Y. Guo, W. Shi, G. Yu, *Adv. Mater.* **2022**, *36*, 2207786.
[5] H. Shan, P. Poredoš, Z. Ye, H. Qu, Y. Zhang, M. Zhou, R. Wang, S. C. Tan, *Adv. Mater.* **2023**, *35*, 2302038.
[6] D. K. Nandakumar, Y. Zhang, S. K. Ravi, N. Guo, C. Zhang, S. C. Tan, *Adv. Mater.* **2019**, *31*, 1806730.
[7] X. Zhang, H. Qu, X. Li, L. Zhang, Y. Zhang, J. Yang, M. Zhou, L. Suresh, S. Liu, S. C. Tan, *Adv. Mater.* **2024**, *36*, 2310219.
[8] N. Hanikel, M. S. Prevot, O. M. Yaghi, *Nat. Nanotechnol.* **2020**, *15*, 348.
[9] W. Song, Z. Zheng, A. H. Alawadhi, O. M. Yaghi, *Nat. Water* **2023**, *1*, 626.
[10] E. Fosso-Kankeu, T. T. I. Nkambule, B. B. Mamba, in *Atmospheric Water Harvesting Development and Challenges*, Springer, Berlin, New York **2023**, Ch 9.
[11] H. Shan, C. Li, Z. Chen, W. Ying, P. Poredos, Z. Ye, Q. Pan, J. Wang, R. Wang, *Nat. Commun.* **2022**, *13*, 5406.
[12] P. Zhang, H. Wang, J. Wang, Z. Ji, L. Qu, *Adv. Mater.* **2023**, *36*, 2303976.
[13] J. Xiao, Z. Liu, K. Kim, Y. Chen, J. Yan, Z. Li, W. Wang, *J. Phys. Chem. C* **2013**, *117*, 23057.
[14] Y. Huang, Q. Yu, M. Li, S. Jin, J. Fan, L. Zhao, Z. Yao, *Chem. Eng. J.* **2021**, *418*, 129474.
[15] C. Anjali, N. K. Renuka, *J. Mater. Res.* **2022**, *37*, 2227.
[16] Y. Song, N. Xu, G. Liu, H. Qi, W. Zhao, B. Zhu, L. Zhou, J. Zhu, *Nat. Nanotechnol.* **2022**, *17*, 857.
[17] H. Guo, Q. Luo, D. Liu, X. Li, C. Zhang, X. He, C. Miao, X. Zhang, X. Qin, *Adv. Mater.* **2024**, *36*, 2414285.
[18] J. Wang, W. Ying, B. Lin, C. Li, C. Deng, H. Zhang, S. Wang, R. Wang, *Adv. Mater.* **2024**, *37*, 2420319.
[19] K. Kordek, L. Jiang, K. Fan, Z. Zhu, L. Xu, M. Al-Mamun, Y. Dou, S. Chen, P. Liu, H. Yin, P. Rutkowski, H. Zhao, *Adv. Energy Mater.* **2018**, *9*, 1802936.
[20] O. L. Li, L. Qin, N. Takeuchi, K. Kim, T. Ishizaki, *Catal. Today* **2019**, *337*, 155.
[21] T. Xu, X. Ding, H. Cheng, G. Han, L. Qu, *Adv. Mater.* **2023**, *36*, 2209661.
[22] J. Xu, T. Li, T. Yan, S. Wu, M. Wu, J. Chao, X. Huo, P. Wang, R. Wang, *Energy Environ. Sci.* **2021**, *14*, 5979.
[23] H. Yao, P. Zhang, Y. Huang, H. Cheng, C. Li, L. Qu, *Adv. Mater.* **2019**, *32*, 1905875.
[24] Z. Li, L. Yu, H. Ma, J. Chen, J. Meng, Y. Wang, Y. Liu, Q. Song, Z. Dong, M. Miao, B. Li, C. Zhi, *Sci. Total Environ.* **2023**, *903*, 166212.
[25] K. Fan, M. Peng, J. Liu, X. Li, X. Wang, B. Kong, X. Liu, *Chem. Eng. J.* **2023**, *461*, 142097.
[26] Z. Zhu, H. Yin, Y. Wang, C. H. Chuang, L. Xing, M. Dong, Y. R. Lu, G. Casillas-Garcia, Y. Zheng, S. Chen, Y. Dou, P. Liu, Q. Cheng, H. Zhao, *Adv. Mater.* **2020**, *32*, 2004670.
[27] K. Kim, P. Y. Zhu, N. Li, X. L. Ma, Y. S. Chen, *Carbon* **2011**, *49*, 1745.
[28] L. Liu, S. Tan, T. Horikawa, D. D. Do, D. Nicholson, J. Liu, *Adv. Colloid Interface Sci.* **2017**, *250*, 64.
[29] F. Deng, Z. Chen, C. Wang, C. Xiang, P. Poredoš, R. Wang, *Adv. Sci.* **2022**, *9*, 2204724.
[30] J. K. Gregory, D. C. Clary, K. Liu, M. G. Brown, R. J. Saykally, *Science* **1997**, *275*, 814.
[31] H. Swenson, N. P. Stadie, *Langmuir* **2019**, *35*, 5409.
[32] W. He, T. Lin, H. Cheng, L. Qu, *Nano Res.* **2023**, *16*, 12491.
[33] L. Liu, Y. Zeng, S. J. Tan, H. Xu, D. D. Do, D. Nicholson, J. Liu, *Chem. Eng. J.* **2019**, *357*, 358.
[34] T. Horikawa, T. Muguruma, D. D. Do, K.-I. Sotowa, J. R. Alcántara-Avila, *Carbon* **2015**, *95*, 137.

© 2025 The Author(s). Advanced Materials published by Wiley-VCH GmbH

[35] X. Chen, N. Yang, Y. Wang, H. He, J. Wang, J. Wan, H. Jiang, B. Xu, L. Wang, R. Yu, L. Tong, L. Gu, Q. Xiong, C. Chen, S. Zhang, D. Wang, *Adv. Mater.* **2021**, *34*, 2107400.
[36] Y. Tao, Q. Wu, C. Huang, W. Su, Y. Ying, D. Zhu, H. Li, *ACS Appl. Mater. Interfaces.* **2022**, *14*, 10966.
[37] Y. F. Yuan, Y. S. Wang, X. L. Zhang, W. C. Li, G. P. Hao, L. Han, A. H. Lu, *Angew. Chem.* **2021**, *133*, 19211.
[38] C. Sun, Y. Zhu, P. Shao, L. Chen, X. Huang, S. Zhao, D. Ma, X. Jing, B. Wang, X. Feng, *Angew. Chem., Int. Ed.* **2023**, *62*, 202217103.
[39] V. T. Nguyen, T. Horikawa, D. D. Do, D. Nicholson, *Carbon* **2014**, *67*, 72.
[40] Y. Hu, Z. Fang, X. Wan, X. Ma, S. Wang, S. Fan, M. Dong, Z. Ye, X. Peng, *Chem. Eng. J.* **2022**, *430*, 133086.
[41] Y. Tao, Q. Wu, C. Huang, D. Zhu, H. Li, *Chem. Eng. J.* **2023**, *451*, 138547.
[42] U. Legrand, D. Klassen, S. Watson, A. Aufoujal, B. Nisol, R. Boudreault, K. E. Waters, J.-L. Meunier, P.-L. Girard-Lauriault, M. R. Wertheimer, J. R. Tavares, *Ind. Eng. Chem. Res.* **2021**, *60*, 12923.
[43] Y. Hanzawa, K. Kaneko, *Langmuir* **1997**, *13*, 5802.
[44] M. Thommes, J. Morell, K. A. Cychosz, M. Fröba, *Langmuir* **2013**, *29*, 14893.
[45] R. Li, Y. Shi, M. Wu, S. Hong, P. Wang, *Nano Energy* **2020**, *67*, 104255.
[46] Y. Song, N. Xu, G. Liu, H. Qi, W. Zhao, B. Zhu, L. Zhou, J. Zhu, *Nat. Nanotechnol.* **2022**, *17*, 857.
[47] S.-Y. Tang, Y.-S. Wang, Y.-F. Yuan, Y.-Q. Ba, L.-Q. Wang, G.-P. Hao, A.-H. Lu, *New Carbon Mater.* **2022**, *37*, 237.
[48] H. Kim, S. Yang, S. R. Rao, S. Narayanan, E. A. Kapustin, H. Furukawa, A. S. Umans, O. M. Yaghi, E. N. Wang, *Science* **2017**, *356*, 430.
[49] F. Fathieh, M. J. Kalmutzki, E. A. Kapustin, P. J. Waller, J. Yang, O. M. Yaghi, *Sci. Adv.* **2018**, *4*, aat3198.
[50] O. A. H. Jones, N. Robinson, *Annu. Rep. NMR Spectrosc.* **2023**, *109*, 29.
[51] B. Maillet, R. Sidi-Boulenouar, P. Coussot, *Langmuir* **2022**, *38*, 15009.
[52] N. Robinson, R. Nasharuddin, E. O. Fridjonsson, M. L. Johns, *Phys. Rev. Lett.* **2023**, *130*, 126204.
[53] S. Dong, L. Liu, N. N. A. Ling, E. F. May, M. L. Johns, N. Robinson, *Langmuir* **2024**, *40*, 16160.
[54] N. Robinson, E. F. May, M. L. Johns, *ACS Appl. Mater. Interfaces.* **2021**, *13*, 54476.
[55] A. Striolo, A. A. Chialvo, P. T. Cummings, K. E. Gubbins, *Langmuir* **2003**, *19*, 8583.
[56] N. Ohta, Y. Nishi, T. Morishita, Y. Ieko, A. Ito, M. Inagaki, *New Carbon Mater.* **2008**, *23*, 216.
[57] A. J. Fletcher, Y. Uygur, K. M. Thomas, *J. Phys. Chem. C* **2007**, *111*, 8349.
[58] S. Picaud, B. Collignon, P. N. M. Hoang, J.-C. Rayez, *Phys. Chem. Chem. Phys.* **2008**, *10*, 6998.
[59] T. C. Kueh, S. H. Chew, A. K. Soh, Y. M. Hung, *Appl. Surf. Sci.* **2023**, *609*, 155414.
[60] Y.-F. Guan, X.-Y. Hong, V. Karanikola, Z. Wang, W. Pan, H.-A. Wu, F.-C. Wang, H.-Q. Yu, M. Elimelech, *Nat. Commun.* **2025**, *16*, 713.
[61] H. Nishiyama, T. Yamada, M. Nakabayashi, Y. Maehara, M. Yamaguchi, Y. Kuromiya, Y. Nagatsuma, H. Tokudome, S. Akiyama, T. Watanabe, R. Narushima, S. Okunaka, N. Shibata, T. Takata, T. Hisatomi, K. Domen, *Nature* **2021**, *598*, 304.
[62] K. Xu, A. Chatzitakis, E. Vøllestad, Q. Ruan, J. Tang, T. Norby, *Int. J. Hydrogen Energy* **2019**, *44*, 587.
[63] J. Rongé, S. Deng, S. Pulinthanathu Sree, T. Bosserez, S. W. Verbruggen, N. Kumar Singh, J. Dendooven, M. B. J. Roeffaers, F. Taulelle, M. De Volder, C. Detavernier, J. A. Martens, *RSC Adv.* **2014**, *4*, 29286.
[64] T. A. Kistler, M. Y. Um, P. Agbo, *J. Electrochem. Soc.* **2020**, *167*, 066502.
[65] G. Zafeiropoulos, H. Johnson, S. Kinge, M. C. M. van de Sanden, M. N. Tsampas, *ACS Appl. Mater. Interfaces.* **2019**, *11*, 41267.
[66] F. Amano, H. Mukohara, H. Sato, C. Tateishi, H. Sato, T. Sugimoto, *Sustainable Energy Fuels* **2020**, *4*, 1443.
[67] G. Heremans, C. Trompoukis, N. Daems, T. Bosserez, I. F. J. Vankelecom, J. A. Martens, J. Rongé, *Sustainable Energy Fuels* **2017**, *1*, 2061.
[68] J. M. Spurgeon, N. S. Lewis, *Energy Environ. Sci.* **2011**, 4, 2993.

© 2025 The Author(s). Advanced Materials published by Wiley-VCH GmbH